Monitoring Ice Nucleation in Pure and Salty Water via High-Speed Imaging and Computer Simulations

Sigurd Bauerecker,*,† Peter Ulbig,‡ Victoria Buch,# Luboš Vrbka,§ and Pavel Jungwirth*,§

Institut für Physikalische and Theoretische Chemie, Technische Universität Braunschweig, D-38106 Braunschweig, Germany, Fachbereich Analytische Messtechnik and Druck, Physikalisch Technische Bundesanstalt, D-38116 Braunschweig, Germany, Fritz Haber Institute for Molecular Dynamics, Hebrew University, Jerusalem, Israel 91904, and Institute of Organic Chemistry and Biochemistry, Academy of Sciences of the Czech Republic and Center for Biomolecules and Complex Molecular Systems, 16610 Prague 6, Czech Republic

Received: December 6, 2007; Revised Manuscript Received: February 7, 2008

High-speed monitoring of the freezing process of freely suspended supercooled pure and salty water droplets is reported for the first time. Combined visual (VIS) and infrared (IR) imaging directly delivers three-dimensional and surface temperature information about the proceeding freezing front with up to 2000 frames per second. The freezing behavior changes gradually up to 1 M and dramatically above a 1 M NaCl concentration. To capture the initial stage of the nucleation molecular dynamics (MD), calculations with atomistic and femtosecond resolution have been performed, and homogeneous ice nucleation in a salt solution has been successfully simulated. A combination of experimental imaging and calculations allows one to unravel structural (e.g., preferred bulk or surface location of the ice nucleus and final ion distribution) and dynamical (time scales for nucleation and freezing) aspects of the freezing process in water and salt solutions. While the thermodynamic consequence of added salt, that is, lowering of the freezing point, is well-known, here, we elucidate the kinetic antifreeze effect of added salt and the molecular origin of the corresponding slow-down of ice nucleation and freezing.

I. Introduction

Ice nucleation in liquid water and aqueous solutions is a common natural process occurring at the ground level seasonally in mid to high latitudes and in the upper troposphere all around the globe.[1] Despite its important role in natural environments and refrigeration technologies, freezing of water is not well understood on a microscopic level from the points of view of structure, dynamics, and the dependence on the degree of supercooling and salinity of the freezing liquid.[1–6] With the aim to address this problem, we present here the concept of experimental and computational "filming" of freezing.

When the supercooling of a neat or salty water sample exceeds a few K, the process of freezing splits into a fast stage and, due to latent heat production, a subsequent slower stage.[1,7] During the fast stage-one freezing (SOF), spongy ice, denoted as stage-one ice (SOI), is formed. It primarily determines the structure of the final ice.[1,7] The second freezing stage is essentially a consolidation process during which the liquid within the SOI matrix solidifies. It is about 100−1000 times slower than the first stage.[1] It is a common practice to influence this freezing process using salts. The effect of added salt is normally viewed in thermodynamic terms as the lowering of the freezing temperature.[1] However, the antifreeze effect of salt can also express itself in the kinetics and dynamics of ice nucleation and freezing, about which little has been known so far at the microscopic level. An extreme example of such a kinetic effect is the action of the fish antifreeze protein which prevents freezing of some arctic fish at subzero seawater temperatures[8] (a small concentration of protein attached to the surface was shown to prevent ice growth[9]). In the present study, we consider a kinetic antifreeze effect of a simpler solute, a normal salt (i.e., NaCl), which we can elucidate with great detail. For that solute, it was possible both to measure and simulate the antifreeze effect and unravel the molecular mechanism. We suggest that this mechanism is likely to be general for the kinetic slow-down effect and applicable also for other solutes.

II. Methods

A. Experimental. An acoustic levitator, high-speed VIS and IR cameras, an illumination device, a humidity meter, a thermometer, and a thermocouple were mounted on an optical desk in the plane of the levitated droplet. All of the equipment was placed into a large cooling chamber and cooled at operating temperatures between −19 and −35 °C. Bidistilled pure water and NaCl (Merck, purity ≥ 99.5%) have been used as neat water and for 0.3, 1, and 3 M salt solutions. Droplets with diameters between 1.5 and 4.5 mm were injected into the middle pressure node of the acoustic field via a sluice in the wall of the cooling chamber. Supercooling temperatures of the suspended droplets have been determined by thermography exploiting the temperature difference between the droplet surface and the directly measured surrounding gas temperature. Nucleation (dominantly at the surface of the droplet) can occur homogeneously,[10] but it can also be initiated by the ultrasonic field[11] or contact with dust particles.

Experimental Components. An ultrasonic levitator[12,13] with a frequency of 20 kHz, a sound radiation power range of 1–11 W, and a preferable sound pressure level of 167 ± 1 dB was

* To whom correspondence should be addressed. For computational materials, E-mail: pavel.jungwirth@uochb.cas.cz. Phone: +420-220 410 314. Fax: +420-220 410 320 (P.V.). For experimental issues, E-mail: s.bauerecker@tu-bs.de (S.B.).

† Technische Universität Braunschweig.

‡ Physikalisch Technische Bundesanstalt.

Hebrew University.

§ Academy of Sciences of the Czech Republic and Center for Biomolecules and Complex Molecular Systems.

10.1021/jp711507f CCC: $40.75
Published on Web 05/15/2008

used. A VIS camera, Photron Fastcam Ultima 512, with frame rates of 500, 1000, and 2000 Hz and IR cameras, (a) Infratec IR 3300, Stirling-cooled MCT detector, frame rates of 300 and 900 Hz and (b) Infratec IR Variocam, microbolometer, 50 Hz, were also utilized. Both cameras were used with germanium objectives, and for camera calibration, integral emissivities of 0.96 and 0.95 were used for water and ice over the spectral range of 8–14 μm.[14,15] The IR and VIS cameras were arranged in an angle of 50°. A Vaisala HMI41 instrument for combined humidity measurement and PT1000 resistance temperature monitoring was used. A 0.25 mm diameter mantle thermocouple for monitoring of local temperature was positioned a few mm apart from the drop surface. A Heraeus/Vötsch VUK 04/500 cooling chamber, dimensions (width × height × depth) 0.76 × 0.89 × 0.77 m^3 = 0.52 m^3, was used, and a heat capacity of a few tens of kilograms of stainless steel ensured the constant temperature of the experiment.

B. Computational. Molecular dynamics simulations of homogeneous nucleation of neat and salty water (with approximate concentrations of 0.3, 0.5, and 0.9 M) were performed in a slab geometry with a unit cell containing 192 water molecules and 1, 2, or 3 sodium and chloride ion pairs. This size is just large enough to provide a slab with a well developed bulk-like region,[16] while small enough to allow for the extremely long simulations needed for capturing homogeneous ice nucleation in salty water. A detailed description of a similar simulation setup for neat water can be found in our recent article.[17] For salty water, simulations of heterogeneous freezing are described in refs 18–20. Here, we prepared slabs of liquid water (with or without added salt) with unit cell dimensions of 15 × 15 × 100 $Å^3$ and two air/water interfaces, the slab thickness being ~30 Å. We used a recent six-center water potential (NE6),[21,22] which has been shown to provide a very reasonable description of the ice/water coexistence with the melting temperature close to that of real water.[22,23] The force field parameters for sodium and chloride were the same as those in our previous study of the heterogeneous freezing of salty water.[18] Up to 1.5 μs simulations with a 1 fs time step were performed at a constant temperature of 250 K (coupling to a thermostat allowed for removal of the excess heat during freezing), and the nucleation events were monitored.

II. Experimental Results

Several approaches exist for the experimental investigation of freezing of smaller water droplets in the micrometer and even nanometer size range, such as those employing electrodynamic Paul traps,[24] free-fall tubes,[25] emulsified droplets,[26] and jet expansions.[27] Here, we employ an alternative method of acoustic levitation (for details, see the Methods section), which is well suited for investigating the freezing (and melting)[12,13] of aqueous droplets up to the millimeter size range.[11,28,29] Compared to droplets hanging on a wire,[30] acoustically suspended droplets are free of wall or substrate contacts. Furthermore, they deform to the first order into shapes characteristic for freely falling raindrops.[31]

For the experimental investigation of freezing in acoustically levitated droplets, we introduce a novel approach which implements the combined IR/VIS high-speed imaging of the results which are presented as a series of snapshots below, as well as complete movies in the Appendix. While high-speed IR imaging during freezing provides a temperature record of the droplet surface, high-speed vis imaging delivers visual information about freezing both at the surface and in the drop interior. These two complementary techniques provide a direct dynamic picture of the freezing processes at the (sub)millisecond time scale and down to a 20 μm resolution. Series of VIS and IR images from the freezing of neat water and salty (1 and 3 M) droplets are presented in Figures 1 and 2. Before going into a detailed analysis of the results, let us summarize the information that can be extracted from these experiments. By simultaneously monitoring the VIS and IR images of the droplets, we can locate the temporal and spatial origin of the newly formed ice nucleus, and by observing the progression of the freezing front, it is possible to extract the freezing rate. Comparing the results for neat and salty droplets also allows us to elucidate the changes in the freezing behavior (i.e., freezing rates, shapes of the freezing front, etc.) connected with added salt.

In the present experiments, the acoustically levitated droplets undergo four cooling phases (Figure 3): (i) liquid droplet cooling, (ii) stage-one freezing, (iii) stage-two freezing, and (iv) solid droplet cooling. For neat water, supercooling temperatures were reached in the range of −19 to −25 °C, with the most common value of −22 °C. During the fast SOF phase (typically less than 40 ms in our experiments with neat water; series A in Figure 1a), the freely suspended droplet has time to release almost no latent heat (less than 1% for neat water) to the gaseous environment, and the droplet can be regarded as a quasi-adiabatic system. These thermal considerations mean that less than a quarter of the mass of a water droplet can be frozen within SOF.[1] Namely, in a first approximation, the fractions of the forming SOI (x) and of the diminishing liquid ($1 - x$) are determined by the specific heat capacities at 0 °C of liquid water, C_{liq} = 4.22 kJ·kg^{-1}·K^{-1}, and ice, C_{ice} = 2.10 kJ·kg^{-1}·K^{-1}, as well as by the droplet temperature increase ΔT = 20 K (which was the maximum observed in our experiments) and the latent heat of melting ΔH_m = 333 kJ·kg^{-1}. The portion x can be derived from the heat balance of the droplet, $x \cdot m \cdot \Delta H_m = x \cdot m \cdot \Delta T \cdot C_{ice} + (1 - x) \cdot m \cdot \Delta T \cdot C_{liq}$, leading to x = 0.225. For ΔT = 25 and 30 K, x values of 0.273 and 0.319 result.

Salty water droplets need more time for SOF, about 100 ms for the 1 M NaCl solution (series B, Figure 1a) and 1000 ms for the 3 M NaCl solution (series C, Figure 1a). In the latter case, the heat transfer out of the droplet cannot be neglected any more. This is consistent with the formation of a distinct icy surface shell in the 3 M solution (series C, Figure 1a, 480 ms). In general, we obtain fractions x of SOI in the range from 10 to 25% of the total mass of the droplet. Note that in all cases, SOI shows a strong enough rigidity to suppress natural oscillations of the droplets. That means that SOI is organized in an interconnected stable network.

The strong temperature gradient between growing SOI and supercooled water and the sudden temperature jump of up to 20 K upon formation of SOI are striking (see Figures 1b and 2). During SOF, temperatures of each of the ice and supercooled water regions were found to be homogeneous within a few tenths of a K, with a sharp boundary in between (Figurs 1b and 2). Temperature gradients at the freezing front were found to be almost constant during freezing, lying in the range of 8−15 K/mm. Also, up to ~1 M, these values do not significantly depend on salt concentration.

It has been reported that surface-dominated nucleation is initiated in the acoustic field.[11] This is consistent with our observation of nucleation starting predominantly at the surface of the neat water droplets. The freezing front during SOF appears mostly planar for neat water and for lower salt concentrations (Figure 1, series A; Figure 4, series G, 58 ms).

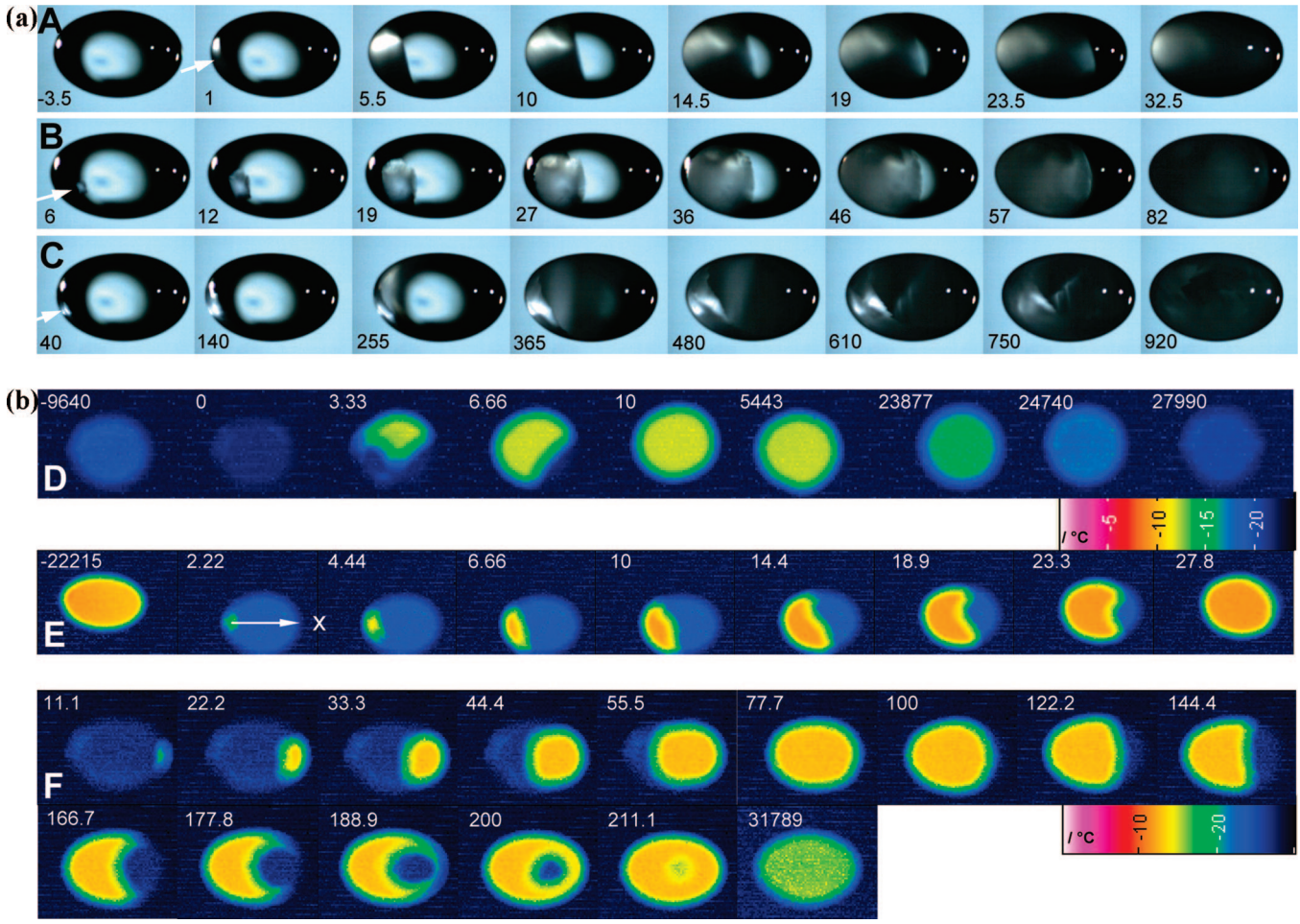

Figure 1. (a) High-speed VIS imaging of the stage-one freezing (SOF) process of acoustically levitated supercooled droplets. The numbers in the frames represent milliseconds after the start of drop freezing. The equatorial droplet diameters were around 4 mm, and the camera time resolution was 0.0005 s/frame in each series. The initial ice nuclei in each series are marked by white arrows. The first frame (−3.5 ms) in series A shows a completely liquid droplet, where all of the light spots are due to illumination (i.e., not due to ice formation). See also the complete movies in the Appendix. Series A (neat water, −24 °C): SOF occurs in a rather plain front which crosses the droplet at a constant growth rate of 0.12 m/s and needs about 34 ms for completion. Series B (1 M NaCl/H_2O solution, −30 °C): SOF occurs as a growing/exploding compact barrel-shaped ice cloud. The freezing growth rate decreases by a factor of 4 compared to that of neat water. Series C (3 M NaCl/H_2O solution, −32 °C): The SOF behavior changes dramatically. The freezing velocity drastically decreases compared to that for the 1 M solution. In most cases, there is a tendency of the salty droplet to freeze as a layer around the surface. Starting from this region, finger- or curtain-shaped ice formations grow toward the interior of the salty drop. (b) High-speed IR imaging of the SOF process of acoustically levitated supercooled droplets. The numbers in the frames are in milliseconds, with zero denoting the start of freezing. The time resolution was 3.33 ms/frame in series D and 1.11 ms/frame in series E and F; the equatorial drop diameters were 2.5, 3.5 and 4.2 mm. The same color scale in °C is used in D and E. Note the strong increase of the surface temperature due to SOF. Series D (neat water, −22 °C): At –9640 ms, the liquid droplet is still a few K above ambient temperature (phase 1). At 0 ms, SOF starts (phase 2). At 10 ms, SOI covers the whole part of the drop facing the camera, and it takes approximately 22 ms to finish SOF. At 5443 ms, the droplet is in the middle of the stage-two freezing (phase 3). At 23877 and 24740 ms, the droplet is completely frozen, cools down (phase 4), and reaches almost ambient temperature at 27990 ms. Series E (neat water, −22 °C): This experiment is comparable with that of series D, but a bigger droplet is used. SOF starts at −19 °C and needs roughly 30 ms. The white arrow in the second frame marks the beginning of the equatorial temperature evolution shown in Figure 2. Series F (1 M NaCl solution, −28 °C): Note that SOF is strongly inhibited in the presence of salt, taking about 220 ms in this case.

In some cases, it is pillow-shaped (Figure 1, series B and series D, 3.33 ms) or changes from convex to concave, which corresponds to a geometrically uneven temperature evolution (Figure 1, series E and Figure 2). On the whole, the freezing front of the droplet gets more corrugated (with a larger surface area) with increasing salinity (Figure 4), in accord with observations in macroscopic samples.[32]

From both IR and VIS imaging, it follows that the growth rate of the forming ice during the SOF process gradually decreases with concentration for up to 1 M salt solutions (Figures 1). For the 3 M salt solution, craggy freezing fronts with curtain-shaped or double-layered ice structures occur (Figure 4). Consequently, no growth rate can be easily determined in this case. However, the growth rate of the ice volume can be estimated from the snapshot sequences. This rate significantly decreases during the typical 1000 ms of freezing time compared to that for less concentrated solutions or pure water. We attribute this behavior to the larger antifreeze impact of the more abundant brine regions, the salt concentration of which increases during freezing. Along the same line, formation of the two nested ice shells (Figure 1, series C, 480 ms; Figure 4, series I) can be rationalized via brine rejection. The shells are comparable in spacing (between 0.5 to 1 mm) and structure to ice plates developing during seawater freezing.[4]

The principal quantitative result extracted from the present experiments is the slow-down of the freezing rate with added salt. The SOI growth rate was found to be 120 mm/s for supercooled (by ∼20 K) neat water droplets. This value agrees

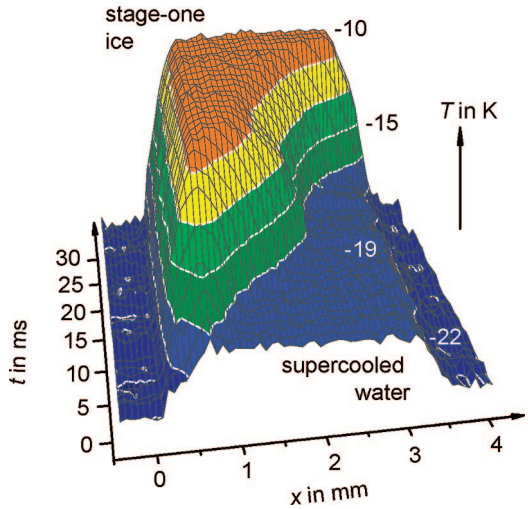

Figure 2. Temperature evolution of the equatorial surface temperature of the freezing neat water droplet shown in Figure 1, series E (see white arrow). Freezing takes place from left to right. During SOF, steep surface temperature gradients of about 10 K/mm build up and the temperatures of both the liquid and SOI remain relatively constant at −19 and −10 °C.

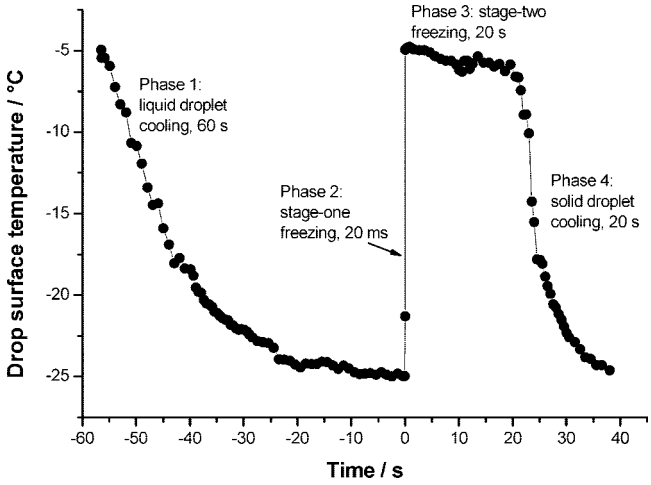

Figure 3. Long-term behavior of the surface temperature of a cooling and freezing acoustically levitated neat water droplet (3 mm diameter) measured by infrared thermography. Phase 1: The liquid droplet cools down from room temperature to the cooling chamber temperature of −25 °C. Phase 2: SOF takes place. It is characterized by a sudden jump in temperature due to latent heat release. SOF is about a thousand times faster than stage-two freezing. Phase 3: Stage-two freezing takes place at an increased temperature level. Here, the liquid water in storage within the SOI network assumedly freezes from the outside to the inside. Phase 4: The completely frozen droplet cools down to ambient temperature at −25 °C. Compared to liquid droplet cooling, this process is faster due to the lower heat capacity of ice. The temperature evolution of these droplets, measured by IR thermography, is similar to that obtained from supercooled freezing droplets hanging on a thermocouple.[30]

well with the upper bound of the free growth velocity diagram of ice in supercooled water ranging from 0 to −18 °C.[1,33] For NaCl solutions, we found significantly smaller SOI growth rates of 30, 20, and 4 mm/s for 0.3, 1, and 3 M solutions, respectively, at around 30 K supercooling. We interpret the observed freezing behavior in salty water as follows. Up to 1 M solution ions are rejected into the brine which encloses the SOI network. The freezing behavior changes between 1 and 3 M. Most of the water molecules are involved in hydration of the Na^+ and Cl^- ions so that formation of the spongy SOI network (which represents

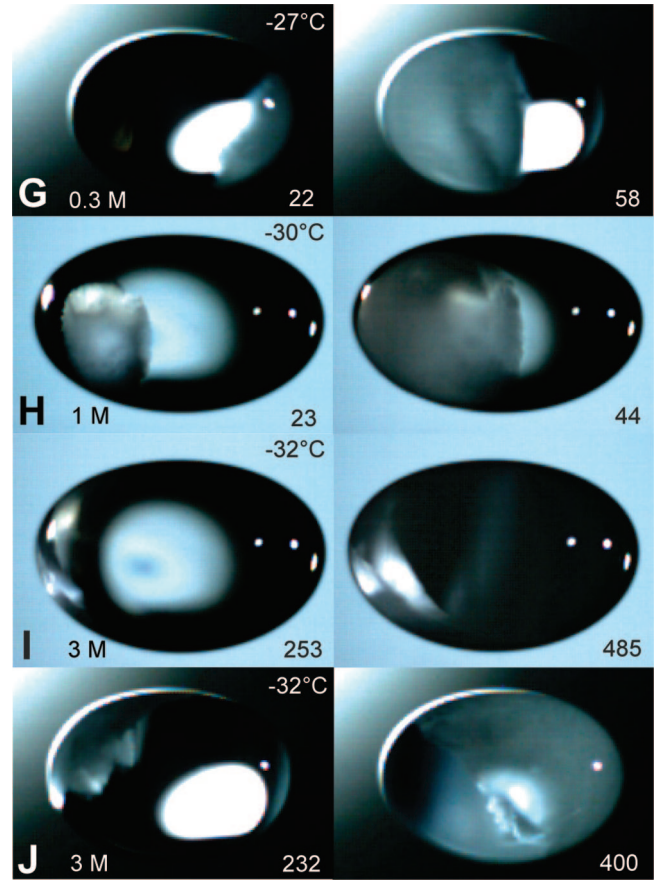

Figure 4. Snapshots of SOF fronts. G, H, I, and J mark the series of frames from different experiments. NaCl salinities, operating temperatures, and times (in ms) after the start of SOF are depicted in the frames. The droplets have equatorial diameters of 2.8, 4.2, 4.0, and 3.0 mm and rotate around the vertical symmetry axis with 13, 8, and 2.5 Hz in G, I, and J but not in H. Note that the harshness of the freezing front increases with salinity. Compare this with the complete movies in the Appendix.

20−30% of the droplet) is suppressed. Thus, during freezing of the 3 M solution, macroscopic brine regions form in the droplet.

III. Computational Results

The experimental results are supported and complemented by molecular dynamics simulations. We report here on the first molecular dynamics simulations of homogeneous ice nucleation in salt solutions. This is a major step forward from our previous simulations of the heterogeneous freezing of salty water in contact with a patch of ice.[18] Even in pure water, homogeneous freezing is a formidable computational task since ice nucleation is an infrequent stochastic event. Salt as an antifreeze agent makes nucleation and freezing more difficult; therefore, very long trajectories are necessary. As a matter of fact, molecular simulations of ice nuclation in neat water have been accomplished for the bulk and open-surface systems only recently,[17,34] while for salt solutions, they have been lacking completely.

By choosing a realistic water model,[21] optimizing the simulation temperature, and performing extremely long simulations, we achieved for the first time homogeneous ice nucleation in an aqueous system with added salt as an antifreeze agent. Successful freezing trajectories were obtained for approximately 0.3, 0.6, and 0.9 M salt solutions, as well as for neat water for

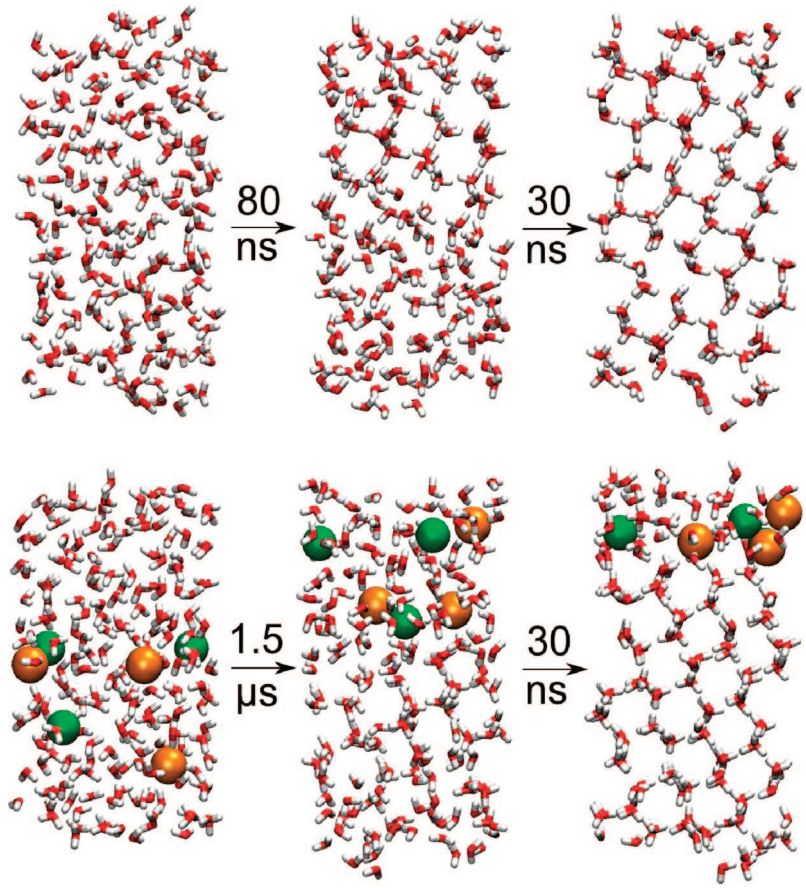

Figure 5. Ice nucleation and homogeneous freezing of a slab of neat water (top) and a 0.9 M aqueous NaCl solution (bottom) represented by snapshots from molecular dynamics simulations. In this MD run, all ions segregated into an unfrozen brine region located at one of two open surfaces of the slab, opposite to that where the ice nucleus formed. Compare this with the complete movies in the Appendix.

comparison. In all cases, the system geometry was a slab with a bulk region in between two air/water interfaces, which allowed investigation of the preferential spatial location of the spontaneously formed ice nucleus. Due to the computationally extremely demanding microsecond nucleation time scales involved, the system size had to be relatively small (192 water molecules and up to 3 Na^+ and Cl^- ions in the unit cell). Such a system size is sufficient for observing the spontaneous formation of the ice nucleus, while for quantitative information about consequent freezing rates, we rely on our previous heterogeneous freezing simulations of neat and salty water employing larger unit cells.[17,18]

Figure 5 shows snapshots from two successful homogeneous ice nucleation simulations without (top) and with (bottom) added salt, the latter at the 0.9 M concentration. In the neat water system, nucleation occurred in the subsurface after about 80 ns. Both the ice nucleus location and time scale of formation are in accord with results of our previous study, where we also outlined possible reasons for the subsurface preference.[17] Upon moving to 0.9 M NaCl, the initiation time became more than an order of magnitude longer, with ice nucleation occurring only around 1.5 μs. One should have in mind that nucleation is a stochastic event with a spread of individual time scales. Nevertheless, for all trajectories (about 10 in total) of systems including salt in the 0.3 – 0.9 M concentration range, spontaneous nucleation took more than one microsecond, while in the comparable neat water system, it always occurred within 100 ns. This is a molecular demonstration of the kinetic antifreeze effect in terms of delayed ice nucleation upon adding salt. As to the newly formed ice nucleus in salt water, analysis of the trajectories shows that, similarly to that for pure water,[17] the driving force for its formation is a local fluctuation (decrease) of ion density at the nucleation spot of a subnanometer size, which can appear either in the (sub)surface or in the bulk.

At this point, a detailed statistical analysis of the formation of the ice nucleus would be in place. However, the relatively small number of successful nuclation trajectories (each of which takes months of CPU time) does not allow for statistically converged information in this respect. Nevertheless, by backtracking trajectories, we attempted to elucidate the time for which water molecules are immobilized before the nucleus forms, both for neat and salty water. An unequivocal result of this analysis is that water molecules involved in the ice nucleus become immobilized several nanoseconds before the actual nucleus forms. Interestingly, within the limited sample of nucleation trajectories, we did not find a clear trend connecting this time (which was always between 1 and 4 ns) with the salt concentration.

Once the ice nucleus is formed, freezing proceeds until, in the case of neat water, the whole system is frozen. In salt solutions, the situation is more complex, with the ions being rejected into an unfrozen surface layer of brine (Figure 5). In the present relatively small systems, where the newly formed ice nucleus occupies a significant part of the system, it takes roughly 30 ns for both neat and salty water to complete the freezing process. To be more quantitative concerning the ice growth process, we have recently performed simulations of the heterogeneous freezing of water and the salt solution in contact with a patch of ice for significantly larger systems with up to 720 water molecules in the unit cell.[18,35] This is computationally

feasible since the cumbersome and time-demanding simulation of the spontaneous formation of the ice nucleus is thus bypassed. These simulations have shown that it takes about twice as long to heterogeneously freeze a 0.3 M NaCl solution compared to that for neat water. This is an additional kinetic antifreeze effect of the added salt, which has been rationalized in terms of ions having to move by random fluctuations away from the freezing front into the unfrozen brine before a new ice layer can grow.[35] Its magnitude is comparable to that extracted from the above experiments.

IV. Conclusions

In summary, we have presented and analyzed real-time snapshots of ice nucleation and the freezing of water and salt solutions. Molecular dynamics simulations provide a detailed picture with atomistic resolution of the freezing events occurring in few nanometer thick aqueous slabs at the nanosecond to microsecond time scale. Homogeneous ice nucleation in a salt solution was successfully simulated for the first time. In a complementary fashion, high-speed IR/VIS imaging provides a dynamical picture of the freezing process in millimeter size levitating aqueous droplets with (sub)millisecond time and 20 μm spatial resolution. The early and later freezing stages are resolved and analyzed for neat water and salt solutions. A series of snapshots demonstrate that salt has both a structural and dynamical (slow-down) effect on the freezing process, particularly at higher concentrations. Computations and experiments show the kinetic antifreeze effect of the added salts both in terms of delayed ice nucleation and slow-down of the early stages of freezing. This observation and its molecular level rationalization provide a new dynamical view on the antifreeze salt effect, complementing thus the traditional thermodynamic understanding in terms of lowering of freezing temperature. The observed change in the freezing behavior with increasing salinity, connected with alteration of ion distribution in the frozen droplets, has potential implications for precipitation dynamics, including the thundercloud electrification phenomenon.[1,36] Our conjecture is that a similar kinetic antifreeze effect is also operative for other solutes. An important example is the fish antifreeze proteins family[8] where, however, the process is more complex since the protein attaches itself strongly to selected spots at the ice surface. Therefore, in contrast to salt solutes, the rejection mechanism does not take place here; therefore, the whole patch of water in the vicinity of the protein becomes inaccessible to freezing.

Acknowledgment. This research was supported by the Czech Ministry of Education (Grant LC512), the Czech granting agency (Grant 203/05/H001), and the Deutsche Forschungsgemeinschaft (Grant 529278). We are grateful to the *META*Centrum in Brno for generous allocation of computer time. L.V. acknowledges financial support from the Japan Foundation for Promotion of Science. We thank U. Block, N. Böse, K. Dinter, G. Hintze, and especially G. Dammass, InfraTec, Inc., and K. Heidkamp for technical support. We appreciate support of R. Tuckermann with calibration data and fruitful discussions with H.K. Cammenga, J. Reichardt, and R. Tuckermann.

Appendix

Five movies of freezing sequences can be downloaded at www.pci.tu-bs.de/agbauerecker/FreezingDrops.

Movie 1: "SeriesA_NeatWaterCompressed.avi" shows the freezing sequence A of Figure 1a (acoustically levitated neat water droplet).

Movie 2: "SeriesB_1molarCompressed.avi" shows the freezing sequence B of Figure 1a (acoustically levitated salty water droplet).

Movie 3: "SeriesJ_3molarCompressed.avi" shows the freezing sequence C of Figure 1a (acoustically levitated high-concentration salty water droplet).

Movie 4: "Simulation_neat.avi" shows the freezing sequence of Figure 5 (top, MD simulation of homogeneous freezing of neat water).

Movie 5: "Simulation_salt.avi" shows the freezing sequence of Figure 5 (bottom, MD simulation of homogeneous freezing of salty water).

The high-resolution versions of the movies are available in the subdirectory "HighResolution".

References and Notes

(1) Pruppacher, H. R.; Klett, J. D. *Microphysics of Clouds and Precipitation*, 2nd ed.; Kluwer: Dordrecht, 1997; Chapter 16 and references therein.
(2) Debenedetti, P. G. *J. Phys.: Condens. Matter* **2003**, *15*, R1669.
(3) Lock, G. S. H. *The Growth and Decay of Ice*; Cambridge University Press: Cambridge, 2005.
(4) Petrenko, V. F.; Whitworth, R. W. *Physics of ice;* Oxford University Press: Oxford, 2006, chapter 12.2 and references therein.
(5) Baker, M. B.; Baker, M. *Geophys. Res. Lett.* **2004**, *31*, L19102.
(6) Ochshorn, E.; Cantrell, W. *J. Chem. Phys.* **2006**, *124*, 54714.
(7) Macklin, W. X.; Ryan, B. F. *J. Atmos. Sci.* **1965**, *22*, 452.
(8) Knight, C. A.; DeVries, A. L.; Oolman, L. D. *Nature* **1984**, *308*, 295.
(9) Kristiansen, E.; Zachariassen, K. E. *Cryobiology* **2005**, *51*, 262.
(10) Tabazadeh, A.; Djikaev, Y. S.; Reiss, H. *Proc. Natl. Acad. Sci. U.S.A.* **2002**, *99*, 15873.
(11) Lü, Y. J.; Xie, W. J.; Wei, B. *Appl. Phys. Lett.* **2005**, *87*, 184107.
(12) Bauerecker, S.; Neidhart, B. *J. Chem. Phys.* **1998**, *109*, 3709.
(13) Bauerecker, S.; Neidhart, B. *Science* **1998**, *282*, 2211.
(14) Schuster, N.; Kolobrodov, V. B. *Infrarotthermographie*; Wiley-VCH: Weinheim, 2004.
(15) Tuckermann, R.; Bauerecker, S.; Cammenga, H. K. *Int. J. Thermophys.* **2005**, *26*, 1583.
(16) Kuo, I. F.-W.; Mundy, C. J. *Science* **2004**, *303*, 658.
(17) Vrbka, L.; Jungwirth, P. *J. Phys. Chem. B* **2006**, *110*, 18126.
(18) Vrbka, L.; Jungwirth, P. *Phys. Rev. Lett.* **2005**, *95*, 148501.
(19) Carignano, M. A.; Baskaran, E.; Shepson, P. B.; Szleifer, I. *Ann. Glaciology* **2006**, *44*, 113.
(20) Carignano, M. A.; Shepson, P. B.; Szlerfier, I. *Chem. Phys. Lett.* **2007**, *436*, 99.
(21) Nada, H.; van der Eerden, J. P.; Furukawa, Y. *J. Cryst. Growth* **2004**, *266*, 297.
(22) Vega, C.; Sanz, E.; Abascal, J. L. F. *J. Chem. Phys.* **2005**, *123*, 144504.
(23) Abascal, J. L. F.; Fernandez, R. G.; Vega, C.; Carignano, M. A. *J. Chem. Phys.* **2006**, *125*, 166101.
(24) Krämer, B.; Hübner, O.; Vortisch, H.; Wöste, L.; Leisner, T.; Schwell, M.; Rühl, E.; Baumgärtel, H. *J. Chem. Phys.* **1999**, *111*, 6521.
(25) Wood, S. E.; Baker, M. B.; Swanson, B. D. *Rev. Sci. Instrum.* **2002**, *73*, 3988.
(26) Koop, T.; Bertram, A. K.; Molina, L. T.; Molina, M. J. *J. Phys. Chem. A* **1999**, *103*, 9042.
(27) Huang, J.; Bartell, L. S. *J. Phys. Chem.* **1995**, *99*, 3924.
(28) Jacob, P.; Stockhaus, A.; Hergenröder, R.; Klockow, D. *Fresenius' J. Anal. Chem.* **2001**, *371*, 726.
(29) Ettner, M.; Mitra, S. K.; Borrmann, S. *Atmos. Chem. Phys* **2004**, *4*, 1925.
(30) Hindmarsh, J. P.; Russell, A. B.; Chen, X. D. *Int. J. Heat Mass Transfer* **2003**, *46*, 1199.
(31) Lupi, V. D.; Hansman, R. J. *J. Atmos. Oceanic Technol.* **1991**, *8*, 541.
(32) Nagashima, K.; Furukawa, Y. *J. Cryst. Growth* **2000**, *209*, 167.
(33) Pruppacher, H. R. *J. Chem. Phys.* **1967**, *47*, 1807.
(34) Matsumoto, M.; Saito, S.; Ohmine, I. *Nature* **2002**, *416*, 409.
(35) Vrbka, L.; Jungwirth, P. *J. Mol. Liq.* **2007**, *134*, 64.
(36) Jungwirth, P.; Rosenfeld, D.; Buch, V. *Atmos. Res.* **2005**, *76*, 190.

JP711507F